

Physiologically-Based Pharmacokinetic Modeling of the Postbiotic Supplement Urolithin A Predicts its Bioavailability Is Orders of Magnitude Lower than Concentrations that Induce Toxicity, but also Neuroprotective Effects

Georg Aichinger,* Maja Stevanoska, Karsten Beekmann, and Shana J. Sturla

Scope: A range of health benefits are attributed to consuming urolithin A (UA), such as improved muscle health, anti-aging activity, and neuroprotection, whereas few studies raise possible adverse effects at high doses, including genotoxicity and estrogenic effects. Therefore, understanding UA bioactivity and safety depends on its pharmacokinetics. However, there is no physiologically-based pharmacokinetic (PBPK) model available for UA, thus limiting reliable assessment of effects observed from in vitro experimentation. **Methods and results:** We characterize glucuronidation rates of UA by human S9 fractions. Partitioning and other physicochemical parameters are predicted using quantitative structure–activity relationship tools. Solubility and dissolution kinetics are determined experimentally. These parameters are used to construct a PBPK model, and results are compared with data from human intervention studies. We evaluate how different supplementation scenarios may influence UA plasma and tissue concentrations. **Concentrations at which either toxic or beneficial effects are previously observed in vitro appear unlikely to be achieved in vivo.** **Conclusion:** A first PBPK model for UA is established. It enables prediction of systemic UA concentrations and is critical for extrapolating in vitro results to in vivo uses. Results support the safety of UA, but also challenge the potential for readily achieving beneficial effects by postbiotic supplementation.


1. Introduction

Urolithins are metabolites that arise from gut microbial transformation of ellagitannins, which are prominently present in fruits like pomegranate and different nuts^[1] (Figure 1). These bacterial metabolites, and in particular urolithin A (UA, Figure 1), are widely regarded to benefit human health. As an antioxidant and inducer of the Nrf2 pathway's anti-inflammatory effects, UA could be responsible for many of the benefits associated with pomegranate consumption.^[2] Based on computational models and animal experiments, it is predicted to pass the blood–brain barrier^[3–5] and was shown to prevent neuroinflammation in the brain of mice.^[6,7] UA was demonstrated to attenuate memory impairment in mice^[6] and is therefore a candidate preventive agent for neurodegenerative diseases.^[8] Also, it was demonstrated to improve the neurological tissue health in mice with traumatic brain injury.^[7] Furthermore, there is ongoing research on UA's potential as an anti-aging bioactive,

with life prolongation demonstrated in *Caenorhabditis elegans*.^[9] Clinical trials describe a positive effect of UA treatment on muscle endurance and health in elderly people^[10] as well as on muscle strength and exercise performance in middle-aged adults.^[11] The proposed underlying mechanism for these effects could be the induction of mitophagy, the self-renewing process of damaged mitochondria.^[2,9]

A major challenge that so far has impeded the therapeutic use of ellagitannin-rich products is interindividual differences in the pharmacokinetics of UA. Its natural formation in the human gut starts with spontaneous hydrolysis as well as tannase-catalyzed hydrolysis of ellagitannins in the stomach and small intestine to quantitatively yield ellagic acid. In approximately 90% of the population, EA can further undergo hydrolytic degradation resulting in the pentahydroxy-dibenzo- α -pyrone, urolithin M5 (UM5). This transformation is proposed to be catalyzed by an as-yet unidentified lactase/decarboxylase enzyme.^[12] From UM5, a range of different urolithins are produced by microbially catalyzed dehydroxylation reactions, resulting in the formation of UA as the most

G. Aichinger, M. Stevanoska, S. J. Sturla
Department of Health Sciences and Technology
ETH Zürich
Zürich 8092, Switzerland
E-mail: georg.aichinger@hest.ethz.ch
K. Beekmann
Wageningen Food Safety Research (WFSR)
Wageningen 6708, the Netherlands

 The ORCID identification number(s) for the author(s) of this article can be found under <https://doi.org/10.1002/mnfr.202300009>

© 2023 The Authors. Molecular Nutrition & Food Research published by Wiley-VCH GmbH. This is an open access article under the terms of the Creative Commons Attribution-NonCommercial-NoDerivs License, which permits use and distribution in any medium, provided the original work is properly cited, the use is non-commercial and no modifications or adaptations are made.

DOI: 10.1002/mnfr.202300009

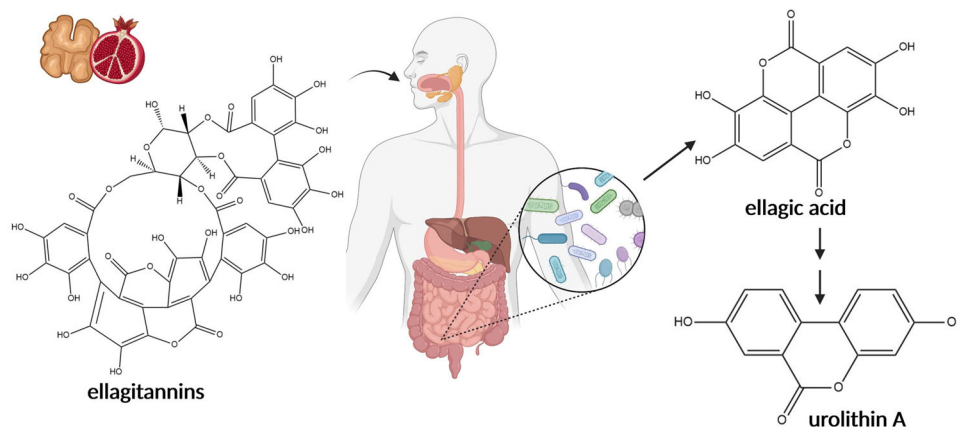


Figure 1. Schematic route of biotransformation of ellagitannins to ellagic acid and urolithin A, including respective chemical structures.

common final metabolite.^[1,12] As this process depends on the function of various microbial enzymes whose occurrence varies amongst individual gut microbiomes, the types of predominantly produced urolithins as well as bioavailable concentrations of UA highly vary between individuals.^[1]

A proposed solution to maximize UA bioavailability while minimizing inter-individual effects is to apply it directly as a post-biotic supplement, rather than relying on its natural formation from ellagitannins. This approach is pursued with the commercial product Mitopure, which has passed standardized clinical safety assessment for repeated doses of 1000 mg per day.^[13,14] An extensive human intervention study conducted by the company that produces Mitopure indicated a more stable bioavailability and less inter-individual fluctuations in plasma concentrations of UA, UA glucuronide (UAGluc), and UA sulfate, when subjects were administered 500 mg of pure UA versus pomegranate juice containing 71 mg ellagitannins and 36 mg EA.^[15] Six hours after administration of UA, average C_{max} values were 0.5 ng mL^{-1} for UA and 481 ng mL^{-1} for UA glucuronide (UAGluc). Mitopure caused no genotoxicity in vivo or mutagenicity in the Ames test, however in vitro concentrations of $23.4 \text{ } \mu\text{g mL}^{-1}$ ($100 \text{ } \mu\text{M}$) UA and higher led to an increase in the percentage of micronucleated cells in human peripheral lymphocytes,^[13] which could be linked to purported UA-induced topoisomerase poisoning at high concentrations.^[16,17] However, it seems highly unlikely that genotoxic concentrations of UA could be reached in the human body, apart from possibly in the gut as the primarily exposed organ. Another potential toxicological concern that was so far not addressed in vivo is the potential endocrine activity of urolithins. Both UA and urolithin B were demonstrated to inhibit 17β -hydroxysteroid dehydrogenase (17β -HSD), an important enzyme involved in the biosynthesis of the sex hormone 17β -estradiol, in a combined in silico/in vitro approach.^[18] The activity towards 17β -HSD and UA's moderate activity as a ligand for estrogen receptors (ER) could potentially lead to a disruption of endocrine processes^[19] if point-of-departure concentrations of urolithins could be reached in target tissues. This makes the elucidation UA pharmacokinetics a pressing matter.

For determining tissue concentrations of chemicals, physiologically-based pharmacokinetic (PBPK) modeling has evolved as a reliable and cost-efficient alternative to animal

testing. This technique uses information on human physiology, physicochemical data, and in vitro metabolism data to predict absorption, distribution, metabolism, and excretion of a compound in a set of stepwise differential equations.^[20] It facilitates the prediction of tissue concentrations, and therefore is used for quantitative in vitro to in vivo extrapolation (QIVIVE).^[21] Thus, it is seen as a cornerstone in international efforts to pursue the 3R's (replacement, reduction, and refinement of animal experiments) in modern pharmacology/toxicology.^[22]

Thus, the aim of this study was to develop a first PBPK model describing tissue concentrations of UA and its primary metabolite after the supplementation of the compound in its pure form. The model was constructed from well-defined human physiological parameters, computed physicochemical parameters for UA and UAGluc, and newly generated experimental data for glucuronidation and dissolution kinetics. The fully parameterized model was evaluated against published human data. Finally, we used the evaluated PBPK model to assess available bioactivity data with regards to both, potential toxicity and beneficial effects of UA. We based it on human physiology that is well described in literature, used computational tools to calculate physicochemical parameters of UA and UAGluc, quantitatively assessed UA glucuronidation kinetics in incubations with intestinal and hepatic S9 fractions and dissolution kinetics under acidic and neutral conditions. Therewith, we parameterized a PBPK model that was evaluated against human data. We then used the model's predictions to perform a first assessment of available in vitro bioactivity data on both, potential toxicity and beneficial effects of UA.

2. Experimental Section

2.1. Chemicals, Reagents and Enzymes

Corning UltraPool Human Liver S9 (mixed gender, 150-donor pool) as well as Corning Gentest UGT Reaction Mix solutions A and B were purchased from Corning (Amsterdam, the Netherlands). Pooled human intestinal S9 fraction was obtained from Biopredic (Saint-Grégoire, France), uridine-5'-diphosphoglucuronic acid (UDPGA) trisodium salt, magnesium chloride, β -glucuronidases (from bovine liver), and sodium acetate from Sigma-Aldrich (Buchs, Switzerland). Alamethicin was

purchased from Enzo Life Sciences AG (Lausen, Switzerland). Urolithin A (3,8-Dihydroxy-6H-benzo[c]chromen-6-one) was obtained from abcr (Karlsruhe, Germany), Urolithin A glucuronide from TRC Canada (Toronto, Canada), DMSO from VWR (Dietikon, Switzerland), 8-octanol and acetonitrile (ACN, HPLC-grade) from Merck-Millipore (Schaffhausen, Switzerland), Tris-HCl from Fluka Chemikals (Buchs, Switzerland).

2.2. HPLC-DAD

The quantitative analysis of UA and UA glucuronide (UAGluc) was carried out on an Agilent 1200 series HPLC instrument using a Waters XBridge BEH130 C18 column (4.6 × 150 mm, 3.5 μm particle size) for separation and a DAD operating at $\lambda = 280$ nm for detection. Eluent A was water (0.1% formic acid) and eluent B was ACN (0.1% formic acid). An isocratic method with 12% eluent B (method 1) was used to detect UA only. For the simultaneous quantification of UA and UAGluc, method 2 was used: 0–3 min, 12% B; 20 min, 25% B; 25 min, 65% B; 28 min, 65% B. Reference standards for UA and UAGluc were used for peak identification and corresponding calibration curves (0.5–100 μM) were made for quantification.

2.3. Glucuronidation by Human Liver S9

Hepatic phase II metabolism was assessed by incubating UA with Corning UltraPool Human Liver S9 in a UDPGA-containing buffer in accordance with the manufacturer's protocol. The S9 reagent (20 mg mL⁻¹ protein) was aliquoted upon delivery and stored at -80 °C until use. For each assay, an aliquot was thawed on ice and Corning Gentest UGT Reaction Mix solutions A and B were used to prepare a reaction solution containing the 1× UGT buffer, 2 mM UDPGA, and 0.5 mg mL⁻¹ S9 protein. 100 μL of each reaction solution were pre-incubated at 37 °C and 350 rpm shaking for 2 min. Incubations without UDPGA were included as a control. UA was dissolved in DMSO and added at a ratio of 1:100, resulting in a final DMSO concentration of 1% v/v and final UA concentrations between 5 and 100 μM. The glucuronidation reaction was stopped after 10 min by addition of 100 μL ACN. Samples were kept at -20 °C for 1 h to allow proteins to precipitate. After centrifugation (10 min, 4 °C, 18 000 × g), the concentrations of UA and UAGluc in the supernatants were determined by HPLC-DAD analysis (method 2). As the two anticipated glucuronides were analytically indistinguishable, they were analyzed as a single peak and the concentration of UAGluc referred to total glucuronide. Curve fitting to Michaelis–Menten kinetics and the calculation of kinetic parameters was performed using the least squares method in Origin 2021.

2.4. Glucuronidation by Small Intestinal S9

To determine the intestinal phase II metabolism of UA, glucuronidation by pooled human intestine S9 (8 mg mL⁻¹ protein) was measured. The incubation mixtures (final volume 160 μL) contained (final concentrations) 10 mM UDPGA in 50 mM Tris-HCl (pH 7.4), 10 mM MgCl₂, and 0.3 mg mL⁻¹ S9 fraction in

0.1 M Tris-HCl (pH 7.4). Prior to adding the substrate, the incubation mixtures were preincubated for 5 min at 37 °C with 25 μg mL⁻¹ alamethicin. To initiate the reaction, UA (concentrations ranging from 10 to 100 μM, added from 100× concentrations in DMSO) was added and the mixtures were incubated for 20 min at 37 °C.

To confirm the formation of glucuronides, 50 μL of the sample was added to 0.1 M sodium acetate (pH 5, 1:1 ratio) containing 1000 units of bovine β-glucuronidases or only 0.1 M sodium acetate as a control. The mixtures were incubated for 1 h at 37 °C. The reactions were terminated by adding a 1:1 ratio of ice-cold methanol. All samples were kept at -20 °C for 2 h to precipitate proteins. Thereafter, the samples were centrifuged (10 min, 4 °C, 16 000 × g) and the supernatants were analyzed by HPLC-DAD. Kinetic parameters for intestinal glucuronidation of UA were determined by fitting these data to the standard Michaelis–Menten equation in Origin 2021 software.

2.5. Solubility and Dissolution of UA

To determine the solubility and dissolution rate of solid UA in the gastrointestinal environment, UA was dissolved in methanol. Different volumes of the resulting solution were pipetted to fresh vials and concentrated to dryness using a miVac duo concentrator. Phosphate buffer (PB; 10 mM Na₂HPO₄, 1.8 mM NaH₂PO₄, pH 7.4) was added to produce a final volume of 1 mL to result in total concentrations between 10 and 200 μM (assuming full solubility). The vials were shaken at 600 rpm and 37 °C for 24 h. Samples were removed after 10, 30, and 60 min, as well as 24 h. These samples were centrifuged (20000 × g, 1 min) and the concentration of UA dissolved in the supernatant was measured by HPLC-DAD (method 1). Dissolution speed was calculated and plotted against theoretic maximal concentrations. Samples taken after 24 h were used to determine maximal solubility in PB. Likewise,^[3] the maximal solubility at acidic conditions was tested in KCl buffer (0.1 mM KCl, 0.02 M HCl, pH 2).

2.6. Determination of LogP and pK_a Values for UA and UAGluc

Octanol–water partitioning of UA (logP = 1.68) and UAGluc (logP = -0.17) was predicted using the KOWWIN v1.68 algorithm.^[23] Other available tools produced varying LogP values for UA (range: 1.68–2.41), therefore, partitioning was experimentally measured by applying the Shake Flask Method.^[24] Briefly, UA was dissolved in methanol (10 mM). A portion of this solution (10 μL) was added to a bilayer of Milli-Q purified water (0.5 mL) and 8-octanol (0.5 mL), resulting in a final concentration of 100 μM. The vial was shaken vigorously for 1 h (1400 rpm, 21 °C), and bilayer was separated by centrifugation (4 min, 8000 × g, 21 °C). The aqueous phase was directly analyzed by HPLC-DAD. The organic phase was evaporated to dryness, reconstituted in 70% methanol, and analyzed by HPLC-DAD. pK_a values of UA (8.0) and UAGluc (3.2) were predicted by PerkinElmer's Chem-Draw.

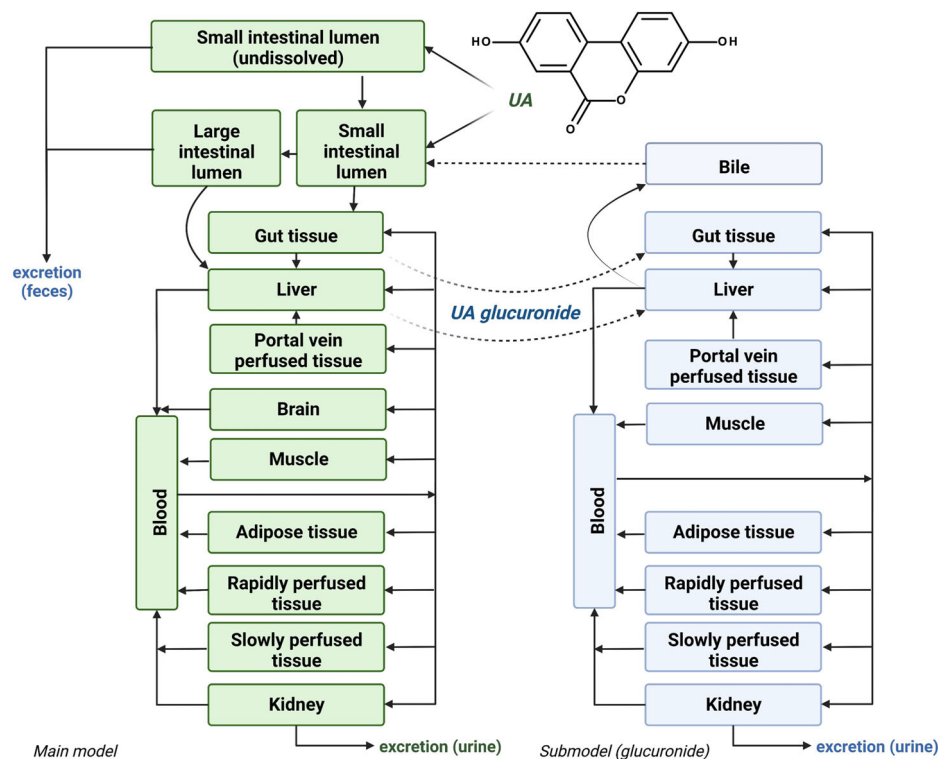


Figure 2. The conceptual PBPK model, with the main model (green) for UA and the submodel (blue) for UA glucuronide, with the dashed lines indicating transfer processes between the two models.

2.7. PBPK Model Conceptualization

As a starting point we used a published model for the gastrointestinal metabolite s-equol.^[25] From its conceptual structure, a PBPK model for UA was further refined in Berkeley Madonna 10 (Figure 2). Gut, muscle, and brain tissue were organs of biological relevance for UA effects, therefore, these were included as dedicated compartments in the model. Furthermore, separate compartments were included for blood, adipose, liver, and kidney tissue. Other organs were grouped as slowly perfused (bone, skin), rapidly perfused (heart, lung), or portal-vein-perfused tissue (spleen, pancreas, colon, stomach). UA was modeled as being taken up via the small intestinal lumen. From there, it was modeled to be transported to the large intestinal lumen and excreted via the feces. A separate compartment was implemented for the non-dissolved fraction of UA in the small intestinal lumen. Uptake of dissolved UA from the small and intestinal lumen was linked to the gut tissue compartment. UA was glucuronidated in small intestinal and liver tissue. Thus, respective links following Michaelis–Menten kinetics were introduced from these compartments to a corresponding compartment in the submodel for UAGluc. This submodel largely mirrored the main model, except for the brain compartment that was irrelevant for UAGluc since the SwissADME tool predicted that the metabolite does not cross the blood–brain barrier.^[3] Urinary excretion was modeled to occur via the kidneys by using the glomerular filtration rate (GFR) as well as the fraction unbound in plasma (fup) as factors describing the clearance velocity.

2.8. Model Parameterization

Data from a recent human intervention study^[15] was to be used to evaluate the PBPK model. The reported values for average bodyweight (BW, 83.3 kg), body mass index (BMI, 29.76), and male/female ratio (32:68) from this study were used to scale the physiology of the virtual model organism (Supporting Information 1) on the basis of published parameters.^[26] Published values for blood volume^[27] and gastrointestinal passage times^[28] were used. Anatomic parameters for the gastrointestinal tract were calculated as previously established.^[29,30] As suggested by Levey et al.,^[31] the mean GFR was set to $125 \text{ mL min}^{-1} (1.73 \text{ m}^2)^{-1}$ and scaled to the body surface area that was calculated from the BW and BMI values reported in the study used for evaluation.^[15] Physico-chemical parameters were calculated based on $\log P$ and pK_a values with the QIVIVE toolbox of Punt et al.^[32] The Berezovsky method^[33] was used to predict tissue partitioning and the method of Lobell and Sivarajah^[34] to predict fup values. Constants for uptake of UA across the small and large intestinal barrier were based on available data from Caco2-transwell permeability experiments^[35] and scaled to in vivo P_{app} values using the algorithm of Sun et al.^[36] Parameters to describe glucuronidation in the liver and small intestine, as well as dissolution kinetics, were measured as described above. Lastly, enterohepatic recirculation (EHR) was included as a factor describing the fraction of UAGluc being excreted via the bile to the small intestinal lumen versus entering the blood stream. After the evaluation of the model based on UA and UAGluc plasma levels after 6 h, the EHR-representing coefficient was increased

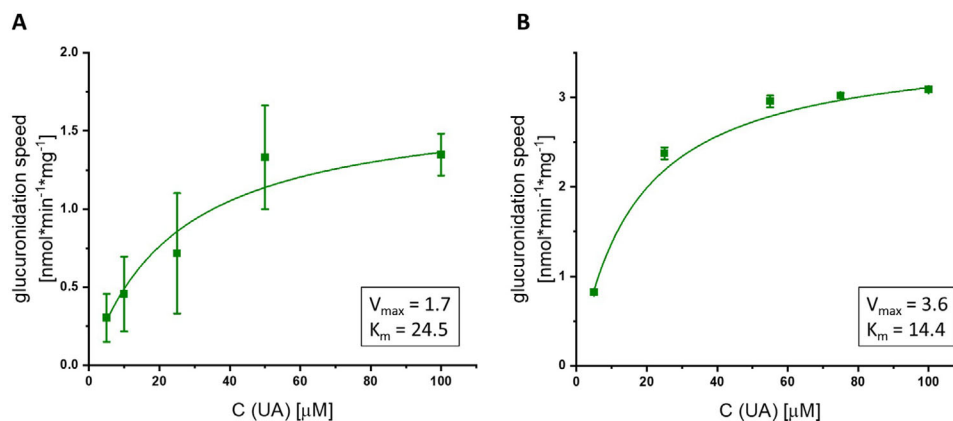


Figure 3. In vitro glucuronidation speed of UA as measured in incubations hepatic (A) and small intestinal (B) S9 fractions. Depicted are the results for the UA-concentration-dependent formation rate of UAGluc in at least three independent experiments, with the green squares representing mean values \pm SEM and the solid lines representing calculated functions for Michaelis–Menten kinetics.

in steps of 0.002 to achieve an optimal matching of the predicted and the in vivo UA plasma concentration at 24 h. All used parameters can be found in the supplied PBPK model code (Supporting Information 2)

2.9. Sensitivity Analysis

A sensitivity analysis was performed to evaluate the impact of parameter deviation on the model's predictions. For this, each parameter was individually increased by 5% and the model was run with a starting dose of 500 mg, matching the oral dose from the primary in vivo study used for model evaluation.^[15] Normalized sensitivity coefficients (SC) were calculated by using the formula developed for this purpose by Evans and Andersen^[37]:

$$SC = \frac{(C' - C)}{(P' - P)} \times \frac{P}{C} \quad (1)$$

Here, C and C' referred to the peak concentration of UA in blood with unchanged parameters or one elevated parameter, respectively, P and P' to the value of the unchanged or elevated parameter of interest.

2.10. Prediction of Tissue Concentrations

The evaluated PBPK model was used to predict UA concentrations in all tissue compartments including the selected tissues of interest (gut, brain, muscle) by simulating three common supplementation scenarios: a) intake of a single dose of 500 and 1000 mg UA and b) repeated intake of 500 or 1000 mg UA once every 24 h for 14 days. C_{\max} and baseline (24 h after application) UA levels were predicted after the last simulated supplementation.

3. Results

3.1. In Vitro Glucuronidation Kinetics

To evaluate the efficiency of UA glucuronidation, the pure compound was incubated with pooled human liver or small intestine

S9 fractions in presence of an excess of UDPGA (Figure 3). Two UA glucuronides were observed as one inseparable peak with the same retention time as the reference standard. Glucuronides were only observed to be formed in presence of UDPGA, but not in the respective control lacking the glucuronic acid donor. Affinity constants for the enzymatic conversion of UA to UAGluc (K_m), calculated by Michaelis–Menten curve fitting using the respective function in Origin 2021, were 24.5 μM (liver) and 14.4 μM (intestine). In vitro V_{\max} values were calculated to be 1.7 $\text{nmol min}^{-1} \text{mg}^{-1}$ hepatic S9 and 3.6 $\text{nmol min}^{-1} \text{mg}^{-1}$ intestinal S9 protein. These values were scaled to the human organism with commonly used scaling factors in PBPK modeling (VLS9 = 107.3 $\text{mg S9 protein g}^{-1} \text{liver}$ ^[38]; VGS9 = 35.2 $\text{mg S9 g}^{-1} \text{small intestine}$ ^[39]). The results suggest rapid glucuronidation of UA to occur in these types of tissue.

3.2. Solubility, Dissolution Kinetics, and Octanol/Water Partitioning

As UA is supplemented as a solid powder, a slow dissolution in the gastrointestinal tract could impact its pharmacokinetic properties. Thus, we determined experimentally that the maximal solubility of UA was similar either at pH 7.4 ($13.0 \pm 0.57 \mu\text{M}$) or pH 2 ($12.6 \mu\text{M}$). Its dissolution speed in PB (pH 7) at 37 °C was clearly concentration-dependent and did not follow a linear dose–speed relationship but rather a Michaelis–Menten-like curve. From the respective curve fit, we calculated the maximal dissolution rate ($22.0 \mu\text{mol L}^{-1} \text{h}^{-1}$) and the half-saturation concentration ($205 \mu\text{mol L}^{-1}$) and those were directly used in the PBPK model (Figure 4). K_{OW} assessment for UA (four experiments) resulted in a measured $\log P$ of 2.11 ± 0.087 .

3.3. PBPK Model Optimization and Evaluation by Comparison to In Vivo Data

Having experimentally determined rates of glucuronidation by hepatic and small intestinal proteins, as well as dissolution kinetics, we conceptualized a PBPK model that included intestinal

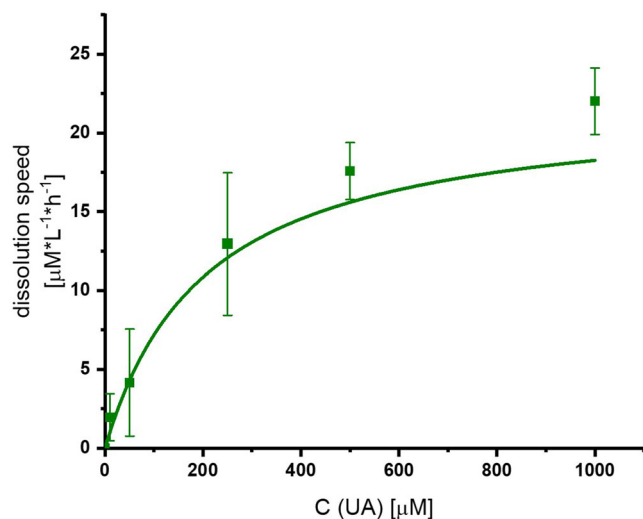


Figure 4. Dissolution speed of UA in phosphate buffer (PB, pH 7.4), at 37 °C and 600 rpm, plotted against the concentration of UA in suspension. Values (green squares) are depicted as means \pm SD of three independent experiments. The line is a fit to the data using the saturation function $y = ax/(b + x)$, with a being maximal dissolution speed and b the half saturation concentration.

dissolution kinetics, passive diffusion across small and large intestinal barriers, small intestinal and hepatic glucuronidation, the distribution of UA and UAGluc across different organs and tissue types, and excretion to urine via the kidneys (Figure 2). To evaluate its accuracy, predicted plasma levels of UA and UAGluc were compared to data from human intervention studies. When an initial round of evaluation against in vivo data for a single ingestion of 500 mg of UA^[15] was performed, the predicted peak times of UA and UAGluc matched the experimental values closely, however C_{\max} values were overestimated by a factor of approximately 10. This problem was solved by including maximal solubility, along with dissolution kinetics, in the stomach and small intestinal lumen compartments. After the reconstruction of dedicated gastrointestinal compartments for the insoluble fraction of UA and the incorporation of the respective parameters, in a second evaluation round, predicted C_{\max} and C_{6h} values

matched closely with in vivo data (Figure 5). However, as a result, the concentration of UA in the blood compartment was severely underestimated at the timepoint of 24 h after exposure. We hypothesized that this was due to EHR, which has been described to occur for UA in an Iberic pig model.^[40] Therefore, to account for the potential influence of EHR on UA bioavailability, an appropriate factor governing this process was estimated by increasing it incrementally in the model and continuously comparing predicted and experimental in vivo C_{24h} values of UA. We found that a coefficient of 0.038 for EHR was optimal (Figure 5). By including this factor, the model predicts 3.8% of UAGluc to be excreted from liver to bile, and subsequently to be recycled via the small intestine. To assess the long-term accuracy of the model including EHR, a second round of evaluation was performed using another set of human data from a study that followed a daily supplementation schedule.^[14] Predicted and reported plasma levels after the seventh day of daily UA supplementation matched very well for both, UA and UAGluc (Table 1). Thus, we hereby supply a first PBPK model for UA that integrates several key factors governing the compound's immediate and chronic bioavailability. The final model code in Berkeley Madonna, including all parameters, is supplied with this publication (Supporting Information 2).

3.4. Sensitivity Analysis

Having established a PBPK model for UA supplementation, we evaluated its sensitivity by varying single parameters with regards to their impact on C_{\max} of UA in blood (Figure 6). The SC for body weight was 1.29, and parameters describing hepatic glucuronidation closely followed (V_{\max} , scaling factor: -0.92 ; affinity constant: 0.96). Similarly, parameters describing blood flow to the liver (QLc; 0.96) and liver volume (VLc; -0.92) were comparably sensitive. Parameters describing uptake across the gastrointestinal barrier had SC values of -0.35 (areaSI, surface area of the small intestinal lumen), 0.24 (areaLI, surface area of the large intestinal lumen), and 0.54 (logPap-pUA, permeability coefficient), and variables accounting for dissolution of solid UA followed with SCs of 0.13 for SOLUA (maximal soluble concentration), 0.84 for V_{\max} UASOL (V_{\max} of UA

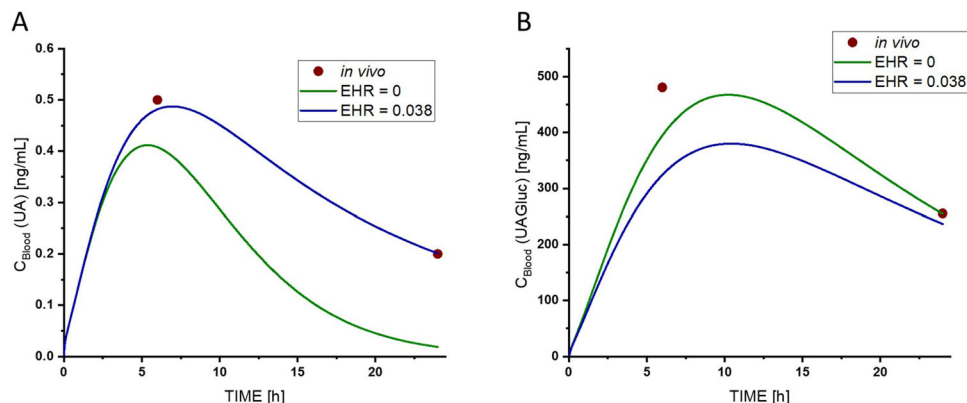


Figure 5. The predicted blood concentrations of UA (A) and its primary human metabolite UAGluc (B) after supplementation with 500 mg UA. Red circles represent mean blood concentrations reported in the recent in vivo study by Singh et al.,^[15] solid lines depict model predictions, either not taking into account enterohepatic recirculation (green) or including an estimated 3.8% EHR of UAGluc (blue).

Table 1. Model evaluation assuming a daily supplementation scenario.

Daily oral dose [mg]	Baseline ^{a)} UA plasma level [nM]		Baseline ^{a)} UAGluc plasma level [nM]	
	Reported in vivo ^[14]	Model prediction	Reported in vivo ^[14]	Model prediction
250	1.2	0.8	800	520
500	1.2	1.3	1200	820
1000	2.0	2.0	1300	1260

^{a)} 24 h after d7 of daily supplementation.

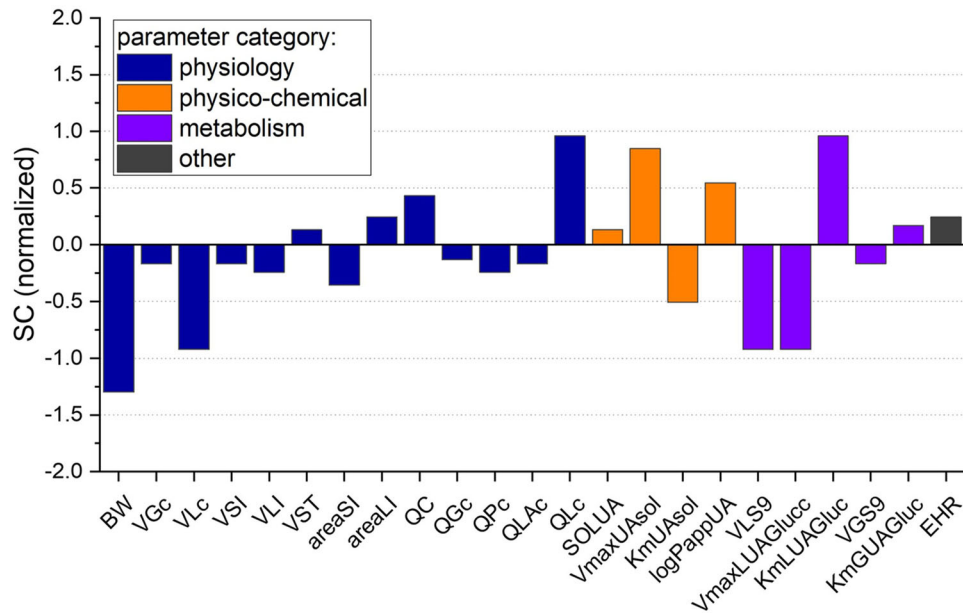


Figure 6. Normalized sensitivity coefficients (SC) calculated from altered C_{max} values (UA, blood) after a 5% elevation of the respective parameter. Parameters with an absolute SC >0.1 are shown. areaSI, surface area of the small intestinal lumen; areaLI, surface area of the large intestinal lumen; BW, bodyweight; EHR, enterohepatic recirculation factor; KmUASOL, affinity constant of UA dissolution; KmGUAGluc, affinity constant for intestinal UA glucuronidation; KmLUAGluc, affinity constant for hepatic UA glucuronidation; logPappUA, logarithm of the permeability coefficient across the intestinal barrier; QC, cardiac output; QGc, relative blood flow to gut tissue; QPc, relative blood flow to portal vein perfused tissue; QLAc, relative blood flow to liver artery; QLC, relative blood flow from the liver; SOLUA, maximum solubility of UA; VGc, relative gut tissue volume; VLc, relative liver tissue volume; VSI, volume of small intestinal lumen; VLI, volume of large intestinal lumen; VST, volume of stomach lumen; VmaxUAsol, maximal velocity of UA dissolution; VLS9, factor to scale S9 protein to liver tissue; VmaxLUAGluc, maximal velocity of hepatic UA glucuronidation; VGS9, factor to scale S9 protein to gut tissue.

dissolution) and -0.51 for KmUASOL (affinity constant of UA dissolution). Thus, bodyweight appears to be the most sensitive parameter, but as anticipated hepatic glucuronidation is closely followed.

3.5. Predicted Concentrations in Tissues of Interest

To predict available concentrations of UA in tissues of biological interest for QIVIVE, the model was run on four supplementation scenarios (500 and 1000 mg dose; single and daily application) to predict respective peak and baseline concentrations (Table 2). Bioavailability was predicted to be 3.8%, with 96.2% of UA being excreted via the feces within the first 24 h after application. The highest concentrations of UA were predicted for gut tissue and under the repeated high dose scenario (C_{max} 40 nM). In all other tissues, including muscle and brain, the model predicted that one-digit nanomolar concentra-

tions at most could be achieved by any supplementation scenario. UAGluc was predicted to reach a C_{max} value of 2.1 μM in plasma in the repeated high dose scenario. These predictions provide a first estimate of achievable tissue concentrations in humans.

4. Discussion

In this study, we built and evaluated a PBPK model that can be used to predict in vivo concentrations of UA and its glucuronides in physiologically relevant tissues. Such a model is required to assess the physiological relevance of biological effects identified from experiments involving in vitro models. The implemented parameters were obtained from literature (human physiology, gastrointestinal permeability), computed by quantitative structure–activity relationship (QSAR) tools (tissue partitioning, plasma binding) or measured in vitro (dissolution kinetics,

Table 2. Predicted tissue concentrations of UA.

	Single dose (day 1)				Repeated dose (day 14)			
	500 mg		1000 mg		500 mg		1000 mg	
	C_{\max}	Baseline	C_{\max}	Baseline	C_{\max}	Baseline	C_{\max}	Baseline
Blood	2.4	0.95	3.5	1.5	3.3	1.3	4.8	2.0
Liver	3.9	1.4	5.5	2.1	5.3	1.8	7.6	2.9
Adipose	3.3	1.5	4.7	2.3	4.5	2.0	6.5	3.1
Gut tissue	42	11	57	18	56	15	77	24
Muscle	2.5	1.0	3.6	1.6	3.5	1.4	5.0	2.2
Brain	5.0	1.9	7.1	3.0	6.9	2.7	9.9	4.2
Slowly perfused tissue	4.4	1.8	6.2	2.8	6.0	2.5	8.7	3.8

^{a)} Concentrations in nmol L⁻¹.

small intestinal and hepatic glucuronidation kinetics). The evaluation of the model by comparison of its predicted plasma concentrations to data from two in vivo pharmacokinetic studies^[14,15] demonstrated its very high accuracy for predicting systemic concentrations of UA and its glucuronide (Figure 2). Sensitivity analysis (Figure 6) revealed bodyweight as the most influential variable impacting the predicted C_{\max} of UA. This confirms the chosen strategy to adapt the physiology of the model to match the population studied in the human intervention study that was primarily used for evaluation. In line with expectations, other influential parameters mostly concerned hepatic metabolism and gastrointestinal solubility.

Glucuronidation of UA was established previously to be the main route of metabolism in humans, while sulfates occur at concentrations that are lower by a factor of approximately 10 lower as compared to the glucuronide.^[15] Thus, we neglected sulfation but quantitatively assessed glucuronidation in subcellular S9 fractions of human liver and small intestine. We found those to rapidly convert UA to UAGluc, following Michaelis–Menten kinetics without substrate inhibition in the tested dose range (1–100 μM). The in vitro K_m and V_{\max} values (Figure 3) were within an order of magnitude of previously published parameters for other polyphenols.^[41,42] In line with calculated SC values (Figure 6), selectively switching off intestinal or hepatic metabolism confirmed the liver as the main organ of UA deactivation by glucuronidation. This suggests that inter-individual differences in circulating UA levels observed after postbiotic supplementation could be attributed to variations in levels or activity of hepatic UDP-glucuronosyltransferase or to differing expression levels of the breast cancer resistance protein that UA is a substrate for^[43] and whose inhibition was demonstrated to prevent UA glucuronidation.^[44]

In preliminary modeling experiments, the model overestimated systemic UA levels by a factor of approximately 10 relative to the available in vivo data,^[15] leading us to discover that the unexpectedly low solubility of the compound in aqueous solutions is a critical factor for its bioavailability. By performing dissolution experiments, we determined a maximal solubility of UA of $13.0 \pm 0.57 \mu\text{M}$ at 37 °C in PB. Moreover, it dissolved at a rather low rate that followed saturation kinetics (Figure 4). Thus, we improved the model by creating a mirror compartment of the

small intestinal lumen to account for a not dissolved fraction of UA in the gut. This adaptation avoided the large overestimation of systemically available UA and lead to a very good fit of PBPK model estimations and in vivo data for both UA and its metabolite UAGluc (Figure 5). This emphasizes the general importance of including dissolution kinetics in PBPK modeling in the case of partially insoluble compounds. Additionally, the importance of solubility for the absorption of dibenzo- α -pyrones could be particularly relevant for kinetic studies on analogous fungal metabolites that are a current research priority in chemical risk assessment.^[45] Furthermore, the strong impact of slow dissolution kinetics on predicted systemic concentrations implies that it might be possible to increase UA bioavailability with alternative formulation methods, such as with pre-solved UA rather than as a powder. Similar efforts have been successfully carried out for its natural precursor ellagic acid.^[46]

In addition to solubility as a critical factor, the PBPK model revealed that there appears to be a significant effect of enterohepatic recirculation on bioavailable levels of UA and UAGluc. Thus, to model not only in vivo C_{\max} values, but also plasma levels 24 h after supplementation, it was essential to include a coefficient describing biliary excretion and enterohepatic recirculation. The occurrence of this process prolongs the systemic half-life of UA as previously demonstrated in an Iberian pig model^[40] and is now corroborated by in silico prediction and comparison with data from a long-term human intervention study^[14] (Table 1).

One main advantage of a PBPK model over a standard in vivo kinetic study is the possibility to predict concentrations specific to tissues of interest. Thus, we simulated a daily intake of UA using a dose strategy suggested for clinical applications and calculated concentrations in various tissues of interest. In line with available data,^[14] repeated intake increased peak and baseline plasma concentrations by about 50 % over a simulation of 14 days. For 1000 mg of UA administered daily, a relatively high dose, C_{\max} concentrations of 4.5, 8.9, and 40 nM were predicted to be reached in muscle, brain, and gut tissue, respectively. Gonad and breast tissue concentrations were not predicted separately due to limitations of the QSAR tools to calculate respective partitioning, but both are expected to align with results for slowly perfused tissue, where a C_{\max} of at most 7.7 nM was predicted. These estimates should serve as reference concentrations for assessing

Table 3. In vitro bioactivity data and corresponding concentrations in comparison to PBPK model—predicted tissue concentrations.

Biological effect	Test system	POD ^{a)}	Predicted C_{\max} ^{b)}
<i>Genotoxicity</i>			
Formation of micronuclei ^[13]	Human peripheral lymphocytes	100 μM	0.0043–0.040
<i>Endocrine activity</i>			
ER- α activation ^[47]	Receptor binding assay	0.44 μM ^{c)}	0.0077
ER-mediated cell growth ^[47]	MCF-7 human breast cancer cells	1 μM	0.0077
Inhibition of 17 β -HSD and reduction of E2 biosynthesis ^[18]	In silico prediction/confirmed in cell-free enzyme inhibition assays and in MCF-7 cells	25 μM	0.0077
<i>Neuroprotection</i>			
Neuroprotective, anti-inflammatory, antiatherogenic ^[48]	Human umbilical vein endothelial cells	10 μM	0.0089
Prevention of glycativ oxidative stress ^[49]	Human neuroblastoma cells	10 μM	0.0089
Prevention of neuroinflammation ^[50]	Murine microglia cells	10 μM	0.0089
Inhibition of A β_{1-42} fibrillation ^[4]	Cell-free	10 μM	0.0089
<i>Muscle health</i>			
Induction of mitophagy ^[9]	<i>C. elegans</i>	10 μM	0.0045
Improvement of muscle endurance, exercise performance, biomarkers of mitochondrial health ^[10,11]	humans	1000 mg d ⁻¹	

a) Point-of departure concentration; b) Maximal tissue concentration after daily intake of 1000 mg UA for 7 days. Concentrations in μM ; c) Exceptionally an IC_{50} value instead of POD.

the potential physiological relevance of bioactivities or potentially hazardous effects observed from in vitro experiments (Table 3).

As an example of a potentially hazardous effect, genotoxicity of UA was observed in a micronucleus assay in human peripheral lymphocytes at 100 μM .^[13] This concentration is more than 2000 times higher than the maximal concentration predicted even in highly exposed gut tissue. Concerning potential adverse effects of UA on the endocrine system, an IC_{50} value of 0.44 μM for ER- α binding and a point-of-departure concentration of 1 μM for ER-mediated cell growth in MCF-7 breast cancer cells was previously reported.^[47] Furthermore, UA was recently reported to inhibit 17 β -HSD, an important enzyme in the biosynthesis of estrogens, at a concentration of 25 μM .^[18] Of note, all these reported concentrations at which endocrine-disruptive effects could potentially occur are several orders of magnitude higher than the predicted maximal concentrations in slowly perfused tissues (Table 3). Thus, results from this study clearly indicate that neither genotoxicity in the gut nor endocrine effects are likely to occur with the suggested dosing of supplementation. Of note, even a drastic increase of the supplemented dose would not lead to toxic concentrations being reached in situ, as the poor solubility limits bioavailability. Therefore, the general assessment of UA as a safe food supplement^[13,14] is confirmed.

While the low bioavailability of UA suggested by the model supports the safe use of UA in supplements, on the other hand, it begs the question of the physiological relevance of beneficial effects reported for UA based on in vitro data. For example, neuroprotective activity, anti-inflammatory, and antiatherogenic effects were reported at a concentration of 10 μM in human umbilical vein endothelial cells,^[48] as was the preventive effect against glycativ oxidative stress in human neuroblastoma cells^[49] or neuroinflammation in murine microglia cells.^[50] Inhibition of A β_{1-42} fibrillation, a preventive effect against Alzheimer's dis-

ease, was also demonstrated at 10 μM .^[4] All these in vitro point of departure (POD) doses for neuroprotection are at least a factor of 1000 above the predicted maximal brain tissue concentrations (Table 2). Furthermore, deglucuronidation in inflamed brain tissue is unlikely to occur based on the predicted lack of capacity of the glucuronide to cross the blood–brain barrier (according to the SwissADME tool^[3]). This suggests that some of the proposed beneficial effects may have little relevance in humans, or at least should be reassessed using much lower concentrations or in long-term human intervention studies.

The situation concerning UA bioavailability in vivo versus observed effects in vitro is somewhat different for the UA-mediated improvement of muscular health, as this effect has been well established in animal experiments^[9,51] and even in clinical trials with elderly people.^[10,15] This suggests that even for high concentration in vitro effects, there may be factors that promote in vivo activities. Intriguingly, the induction of mitophagy as the proposed underlying mechanism was demonstrated at concentrations starting from 10 μM .^[9] These seem far from being achievable in muscle tissue according to the PBPK model with a C_{\max} of 4.5 nM in the high dose—repeated intake scenario. Possible explanations for this discrepancy could be low-dose effects of chronic UA exposure or a tissue-specific occurrence of deglucuronidation. UAGluc is predicted to reach concentrations of 2.1 μM in plasma and 1.1 μM in skeletal muscles with the scenario of chronic intake of 1000 mg day⁻¹. The activity of β -glucuronidase, the enzyme responsible for tissue deglucuronidation phenomena, is increased with lactate secretion due to dysfunctional mitochondria^[52,53] and might thus be particularly high in muscle tissue of patients already suffering from impaired mitochondrial health due to age or disease. If the dependence of mitophagy-inducing effects of UA from β -glucuronidase would be confirmed, this could have broad implications for its use

as a nutraceutical. For example, lactate secretion is commonly known as a side effect of physical activity,^[54] and one might thus speculate that combined UA supplementation with physical activity could improve outcomes. Furthermore, a co-supplementation of UA with lactate could also be explored as an approach to increase the induction of mitophagy by UA. It would be further relevant to expand this PBPK model to incorporate the metabolic formation of UA from ellagitannins by including a compartment describing microbial transformation in the intestinal lumen, based on previously established techniques.^[25,29,41] This would facilitate a direct comparison of the two routes of exposure regarding achievable tissue concentrations, and thus bioactivity.

Taken together, this PBPK-modeling and QIVIVE approach clarified open questions about the safety of UA and delivered predicted tissue concentrations, which can be used to assess the likelihood for the in vivo occurrence of proposed biological effects.

5. Conclusion

We hereby described and evaluated a PBPK model for the post-biotic supplementation of UA that is ready to use for QIVIVE. Solubility and enterohepatic recirculation are confirmed to be key contributing factors to UA pharmacokinetics, which could be relevant concerning safety and efficacy of many more natural products. First insights concerning tissue-of-interest concentrations reveal low nanomolar peak concentrations in most tissues. A comparison with available in vitro data indicates that toxic effects exerted by UA are highly unlikely to occur, but also challenges the in vivo relevance of some proposed beneficial effects.

Supporting Information

Supporting Information is available from the Wiley Online Library or from the author.

Acknowledgements

This research was supported as a fellowship by the Future Food Initiative, a program run by the World Food System Center of ETH Zurich, the Integrative Food and Nutrition Center of EPFL and their industry partners.

Open access funding provided by Eidgenössische Technische Hochschule Zurich.

Conflict of Interest

The authors declare no conflict of interest.

Author Contributions

G.A. was involved in study design, acted as the main project supervisor, executed experiments, constructed and refined the PBPK model, analyzed the data, and wrote the initial manuscript. M.S. executed intestinal S9 incubation experiments, contributed the corresponding paragraph in the Experimental Section and refined the manuscript. K.B. was involved in study design, acted as a consultant for PBPK modeling and refined the manuscript. S.J.S. was involved in study design, project supervision, and refined the manuscript.

Data Availability Statement

The data that support the findings of this study are available from the corresponding author upon reasonable request.

Keywords

ADME, nutraceutical, PBPK, polyphenol, QIVIVE

Received: January 6, 2023

Revised: April 24, 2023

Published online: June 13, 2023

- [1] F. A. Tomás-Barberán, A. González-Sarrías, R. García-Villalba, M. A. Núñez-Sánchez, M. V. Selma, M. T. García-Conesa, J. C. Espín, *Mol. Nutr. Food Res.* **2017**, *61*, 1500901.
- [2] D. D'Amico, P. A. Andreux, P. Valdés, A. Singh, C. Rinsch, J. Auwerx, *Trends Mol. Med.* **2021**, *27*, 687.
- [3] A. Daina, O. Michielin, V. Zoete, *Sci. Rep.* **2017**, *7*, 42717.
- [4] T. Yuan, H. Ma, W. Liu, D. B. Niesen, N. Shah, R. Crews, K. N. Rose, D. A. Vatter, N. P. Seeram, *ACS Chem. Neurosci.* **2016**, *7*, 26.
- [5] M. Kujawska, M. Jourdes, M. Kurpik, M. Szulc, H. Szafer, P. Chmielarz, G. Kreiner, V. Krajka-Kuźniak, P. Ł. Mikołajczak, P.-L. Teissedre, J. Jodynis-Liebert, *Int. J. Mol. Sci.* **2020**, *21*, 202.
- [6] Z. Gong, J. Huang, B. Xu, Z. Ou, L. Zhang, X. Lin, X. Ye, X. Kong, D. Long, X. Sun, X. He, L. Xu, Q. Li, A. Xuan, *J. Neuroinflammation* **2019**, *16*, 62.
- [7] Q. Y. Gong, L. Cai, Y. Jing, W. Wang, D. X. Yang, S. W. Chen, H. L. Tian, *Neural Regen. Res.* **2022**, *17*, 2007.
- [8] D. P. W. Jayatunga, E. Hone, H. Khaira, T. Lunelli, H. Singh, G. J. Guillemin, B. Fernando, M. L. Garg, G. Verdile, R. N. Martins, *Nutrients* **2021**, *13*, 3744.
- [9] D. Ryu, L. Mouchiroud, P. A. Andreux, E. Katsyuba, N. Moullan, A. A. Nicolet-Dit-Félix, E. G. Williams, P. Jha, G. Lo Sasso, D. Huzard, P. Aebischer, C. Sandi, C. Rinsch, J. Auwerx, *Nat. Med.* **2016**, *22*, 879.
- [10] S. Liu, D. D'Amico, E. Shankland, S. Bhayana, J. M. Garcia, P. Aebischer, C. Rinsch, A. Singh, D. J. Marcinek, *JAMA Netw. Open* **2022**, *5*, e2144279.
- [11] A. Singh, D. D'Amico, P. A. Andreux, A. M. Fouassier, W. Blanco-Bose, M. Evans, P. Aebischer, J. Auwerx, C. Rinsch, *Cell Rep. Med.* **2022**, *3*, 100633.
- [12] A. Cortés-Martín, R. García-Villalba, A. González-Sarrías, M. Romo-Vaquero, V. Loria-Kohen, A. Ramírez-de-Molina, F. A. Tomás-Barberán, M. V. Selma, J. C. Espín, *Food Funct.* **2018**, *9*, 4100.
- [13] J. Heilman, P. Andreux, N. Tran, C. Rinsch, W. Blanco-Bose, *Food Chem. Toxicol.* **2017**, *108*, 289.
- [14] P. A. Andreux, W. Blanco-Bose, D. Ryu, F. Burdet, M. Ibberson, P. Aebischer, J. Auwerx, A. Singh, C. Rinsch, *Nat. Metab.* **2019**, *1*, 595.
- [15] A. Singh, D. D'Amico, P. A. Andreux, G. Dunngalvin, T. Kern, W. Blanco-Bose, J. Auwerx, P. Aebischer, C. Rinsch, *Eur. J. Clin. Nutr.* **2022**, *76*, 297.
- [16] G. Aichinger, *Int. J. Mol. Sci.* **2021**, *22*, 13063.
- [17] V. Furlanetto, G. Zagotto, R. Pasquale, S. Moro, B. Gatto, *J. Agric. Food Chem.* **2012**, *60*, 9162.
- [18] L. Dellaflora, M. Milioli, A. Falco, M. Interlandi, A. Mohamed, M. Frotscher, B. Riccardi, P. Puccini, D. D. Rio, G. Galaverna, C. Dall'Asta, *Mol. Nutr. Food Res.* **2020**, *64*, 2000289.
- [19] R. Vini, J. M. Azeez, V. Remadevi, T. R. Susmi, R. S. Ayswarya, A. S. Sujatha, P. Muraleedharan, L. M. Lathika, S. Sreeharshan, *Front. Nutr.* **2022**, *8*, 800990.
- [20] I. M. C. M. Rietjens, J. Lousse, A. Punt, *Mol. Nutr. Food Res.* **2011**, *55*, 941.

- [21] A. Punt, H. Bouwmeester, B. J. Blaauboer, S. Coecke, B. Hakkert, D. F. G. Hendriks, P. Jennings, N. I. Kramer, S. Neuhoff, R. Masereeuw, A. Paini, A. Peijnenburg, M. Rooseboom, M. L. Shuler, I. Sorrell, B. Spee, M. Strikwold, A. D. Van der Meer, M. Van der Zande, M. Vinken, H. Yang, P. M. J. Bos, M. B. Heringa, *ALTEX* **2020**, *37*, 607.
- [22] D. Krewski, M. E. Andersen, M. G. Tyshenko, K. Krishnan, T. Hartung, K. Boekelheide, J. F. Wambaugh, D. Jones, M. Whelan, R. Thomas, C. Yauk, T. Barton-Maclaren, I. Cote, *Arch. Toxicol.* **2019**, *94*, 1.
- [23] OECD, US Environmental Protection Agency, Log Kow in Parameters, 2D in OECD QSAR Toolbox v.4.2, KOWWIN v1.68 **2012**.
- [24] OECD, Test No. 107: Partition Coefficient (n-octanol/water): Shake Flask Method, **1995**.
- [25] Q. Wang, B. Spengelink, R. Boonpawa, I. M. C. M. Rietjens, K. Beekmann, *Mol. Nutr. Food Res.* **2020**, *64*, e1900912.
- [26] S. Willmann, K. Höhn, A. Edginton, M. Sevestre, J. Solodenko, W. Weiss, J. Lippert, W. Schmitt, *J. Pharmacokinet. Pharmacodyn.* **2007**, *34*, 401.
- [27] R. P. Brown, M. D. Delp, S. L. Lindstedt, L. R. Rhomborg, R. P. Beliles, *Toxicol. Ind. Health* **1997**, *13*, 407.
- [28] Y. T. Wang, S. D. Mohammed, A. D. Farmer, D. Wang, N. Zarate, A. R. Hobson, P. M. Hellström, J. R. Semler, B. Kuo, S. S. Rao, W. L. Hasler, M. Camilleri, S. M. Scott, *Aliment. Pharmacol. Ther.* **2015**, *42*, 761.
- [29] D. M. Mendez-Catala, Q. Wang, I. M. C. M. Rietjens, *Mol. Nutr. Food Res.* **2021**, *65*, 2100443.
- [30] A. Geliebter, S. A. Hashim, *Physiol. Behav.* **2001**, *74*, 743.
- [31] A. S. Levey, L. A. Inker, J. Coresh, *Am. J. Kidney Dis.* **2014**, *63*, 820.
- [32] A. Punt, N. Pinckaers, A. Peijnenburg, J. Louisse, *Chem. Res. Toxicol.* **2021**, *34*, 460.
- [33] L. M. Berezhkovskiy, *J. Pharm. Sci.* **2004**, *93*, 1628.
- [34] M. Lobell, V. Sivarajah, *Mol. Divers* **2003**, *7*, 69.
- [35] R. García-Villalba, H. Vissenaekens, J. Pitart, M. Romo-Vaquero, J. C. Espín, C. Grootaert, M. V. Selma, K. Raes, G. Smagghe, S. Possemiers, J. Van Camp, F. A. Tomas-Barberan, *J. Agric. Food Chem.* **2017**, *65*, 5480.
- [36] D. Sun, H. Lennernas, L. S. Welage, J. L. Barnett, C. P. Landowski, D. Foster, D. Fleisher, K. D. Lee, G. L. Amidon, *Pharm. Res.* **2002**, *19*, 1400.
- [37] M. V. Evans, M. E. Andersen, *Toxicol. Sci.* **2000**, *54*, 71.
- [38] X. Wang, B. He, J. Shi, Q. Li, H.-J. Zhu, *Drug Metab. Dispos.* **2020**, *48*, 31.
- [39] S. A. Peters, C. R. Jones, A. L. Ungell, O. J. Hatley, *Clin. Pharmacokinet.* **2016**, *55*, 673.
- [40] J. C. Espín, R. González-Barrio, B. Cerdá, C. López-Bote, A. I. Rey, F. A. Tomás-Barberán, *J. Agric. Food Chem.* **2007**, *55*, 10476.
- [41] Q. Wang, B. Spengelink, R. Boonpawa, I. Rietjens, *J. Agric. Food Chem.* **2022**, *70*, 343.
- [42] R. Boonpawa, A. Spengelink, I. M. C. M. Rietjens, A. Punt, *Biochem. Pharmacol.* **2014**, *89*, 287.
- [43] A. González-Sarrías, V. Miguel, G. Merino, R. Lucas, J. C. Morales, F. Tomás-Barberán, A. I. Alvarez, J. C. Espín, *J. Agric. Food Chem.* **2013**, *61*, 4352.
- [44] A. González-Sarrías, J. A. Giménez-Bastida, M. Á. Núñez-Sánchez, M. Larrosa, M. T. García-Conesa, F. A. Tomás-Barberán, J. C. Espín, *Eur. J. Nutr.* **2014**, *53*, 853.
- [45] G. Aichinger, G. Del Favero, B. Warth, D. Marko, *Compr. Rev. Food Sci. Food Saf.* **2021**, *20*, 4390.
- [46] G. Zuccari, S. Baldassari, G. Ailuno, F. Turrini, S. Alfei, G. Caviglioli, *Appl. Sci.* **2020**, *10*, 3353.
- [47] M. Larrosa, A. González-Sarrías, M. T. García-Conesa, F. A. Tomás-Barberán, J. C. Espín, *J. Agric. Food Chem.* **2006**, *54*, 1611.
- [48] L. Mele, P. Mena, A. Piemontese, V. Marino, N. López-Gutiérrez, F. Bernini, F. Brighenti, I. Zanotti, D. Del Rio, *Arch. Biochem. Biophys.* **2016**, *599*, 42.
- [49] E. Verzelloni, C. Pellacani, D. Tagliacuzzi, S. Tagliaferri, L. Calani, L. G. Costa, F. Brighenti, G. Borges, A. Crozier, A. Conte, D. Del Rio, *Mol. Nutr. Food Res.* **2011**, *55*, S35.
- [50] N. A. DaSilva, P. P. Nahar, H. Ma, A. Eid, Z. Wei, S. Meschwitz, N. H. Zawia, A. L. Slitt, N. P. Seeram, *Nutr. Neurosci.* **2019**, *22*, 185.
- [51] P. Luan, D. D'Amico, P. A. Andreux, P.-P. Laurila, M. Wohlwend, H. Li, T. Imamura de Lima, N. Place, C. Rinsch, N. Zanou, *J. Auwerx, Sci. Transl. Med.* **2021**, *13*, eabb0319.
- [52] Y. Kawai, *J. Clin. Biochem. Nutr.* **2014**, *54*, 145.
- [53] A. Ishisaka, K. Kawabata, S. Miki, Y. Shiba, S. Minekawa, T. Nishikawa, R. Mukai, J. Terao, Y. Kawai, *PLoS One* **2013**, *8*, e80843.
- [54] G. A. Brooks, in *Circulation, Respiration, and Metabolism* (Ed:R. Gilles), Springer, Berlin, Heidelberg **1985**, pp. 208–218.